The 2020 World Congress on
Advances in Civil, Environmental, & Materials Research (ACEM20)
25-28, August, 2020, GECE, Seoul, Korea

Modeling of tornado vortex and its effects on low-rise and tall buildings

*YC Kim[1)] and Y Tamura[2)]

[1)] *Department of Architecture, Tokyo Polytechnic University, Atsugi, 2430297, Japan.*
[2)] *School of Civil Engineering, Chongqing University, Chongqing, 400045, China.*
[1)] kimyc@arch.t-kougei.ac.jp

ABSTRACT

Tornadoes are the most devastating meteorological natural hazards and are generally defined as violently rotating columns of air, pendant from the base of a convective cloud and often observable as funnel cloud attached to a cloud base. Parameters affecting the structure of a tornado vortex include swirl ratio, (radial) Reynolds number, surface roughness, and translational movement.

Besides field measurements, indoor experiments and computational simulations, many theoretical and empirical numerical models have been proposed for preliminary tornado-resistant design of buildings and structures. Numerical models include the modified Rankine model, the Burgers-Rott model, the Kuo-Wen model, and the Baker model. The idealized and inviscid modified Rankine model has been widely used as a first approximation. Numerical models should explain the physical structure of tornado vortices, but there are many weaknesses in existing numerical models in their physical understanding.

The present paper proposes a new empirical model for a one-cell tornado vortex, and its loading effects induced by surface pressures on low-rise building and aerodynamic forces on a tall building are calculated and compared with those from existing numerical models. Peak normal stress in column on low-rise building from the proposed model show the intermediate value and trend when compared with the existing models, and the aerodynamic forces on a tall building obtained from the proposed model show similar values to most existing models, although those from the Baker model show much larger values.

1. INTRODUCTION

Tornadoes are the most devastating meteorological natural hazards and are generally defined as violently rotating columns of air, pendant from the base of a convective cloud and often observable as funnel cloud attached to a cloud base. Tornadoes can be characterized by three orthogonal velocity components, radial U,

---

[1)] Professor
[2)] Professor

tangential V and vertical W, as shown in Fig.1, and the main findings on the structure of a tornado vortex can be summarized as follows (Kim and Matsui, 2017). Parameters affecting the structure of a tornado vortex include swirl ratio, (radial) Reynolds number, surface roughness, and translational movement. The effect of increasing swirl ratio on tornado structure is well known, i.e., as swirl ratio increases, tornado vortices evolve from a one-cell vortex to multiple vortices. Reynolds number seems to have little effect on tornado vortices if it is larger than a certain critical value. Introducing surface roughness equivalent to that of a city center has an overall effect similar to reducing swirl ratio. For velocity components, radial inflow is found to exist up to hundreds of meters from the tornado center, but the strongest inflow is concentrated very near the ground, implying a variation of vertical profile of radial.

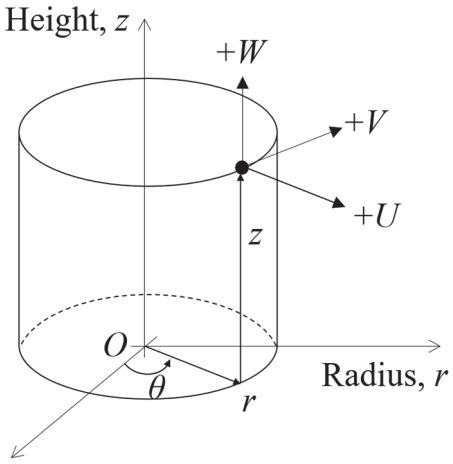

Fig.1 Definition of velocity components.

Continued devastation of buildings and structures results largely from a lack of understanding of interactions between tornadoes and their aerodynamic forces on structures. To precisely evaluate tornado-induced loads, three loading cases should be considered (Baker, 2016). First is loads directly related to the flow over the structure resulting in time-varying surface pressure. Second is loads due to differences in the rapidly changing low pressure near the tornado core and resulting pressure changes around/within buildings. Last is loads induced by wind-borne debris. The second and third cases are usually ignored in wind-resistant design of buildings and structures under synoptic wind.

Besides field measurements, wind tunnel experiments and computational simulations, many theoretical and empirical numerical models have been proposed for preliminary tornado-resistant design of buildings and structures. Numerical models include the modified Rankine model, the Burgers-Rott model, and the Kuo-Wen model. Most recently, Baker (2016) proposed empirical models of one- and two-cell tornado vortices.

The present paper proposes a new empirical modeling for a tornado vortex in an attempt to overcome the shortcomings of existing numerical models. To determine the potential application of the proposed model to current codes and standards, its loading effects induced by surface pressures on low-rise building and aerodynamic

force coefficients on tall building were calculated and compared with those obtained from existing numerical models. Aerodynamic force coefficients on tall building were considered to clearly examine the effect of vertical profile of velocity components as well as possible damages of tall buildings in the large downtown area.

2. NUMERICAL MODELS USED IN THE PRESENT STUDY

When tornado vortices with the following properties (a) ~ (d) are considered, the normalized momentum equations and normalized mass conservation equation for an inviscid and incompressible flow in cylindrical coordinates (r, θ, z) are Equations (1) ~ (5). In the present study, the viscosity term was neglected because the Reynolds number of real tornadoes is high enough (Church et al., 1979).

(a) Time independent (steady-state) i.e., ∂/∂t = 0.
(b) Axisymmetric i.e., ∂/∂θ = 0.
(c) Pressure distribution depends on radial and vertical directions only, i.e., P = f(r, z).
(d) No body forces, i.e., Fr = Fθ = Fz = 0.

Radial momentum equation:

$$\bar{U}\frac{\partial \bar{U}}{\partial \bar{r}} + \frac{\bar{W}}{\zeta}\frac{\partial \bar{U}}{\partial \bar{z}} - \frac{\bar{V}^2}{\bar{r}} = -\frac{\partial \bar{P}}{\partial \bar{r}} \quad (1)$$

Tangential momentum equation:

$$\bar{U}\frac{\partial \bar{V}}{\partial \bar{r}} + \frac{\bar{W}}{\zeta}\frac{\partial \bar{V}}{\partial \bar{z}} + \frac{\bar{U}\bar{V}}{\bar{r}} = 0 \quad (2)$$

Vertical momentum equation:

$$\zeta\bar{U}\frac{\partial \bar{W}}{\partial \bar{r}} + \bar{W}\frac{\partial \bar{W}}{\partial \bar{z}} = -\frac{\partial \bar{P}}{\partial \bar{z}} \quad (3)$$

Mass conservation equation:

$$\frac{\partial \bar{U}}{\partial \bar{r}} + \frac{1}{\zeta}\frac{\partial \bar{U}}{\partial \bar{z}} + \frac{\bar{U}}{\bar{r}} = 0 \quad (4)$$

$$\zeta = \frac{z_{ref}}{r_{ref}} \quad (5)$$

where, ¯ means normalized quantity: all the velocity components were normalized by a reference velocity Uref, radial distance was normalized by a reference radius rref, and height was normalized by a reference height zref. P is static pressure normalized by ρUref2, ρ is air density, and t is time. Fr, Fθ, and Fz are body forces in the r, θ, and z directions, respectively, which were ignored in the present study for simplicity (Baker, 2016). Note that reference velocity Uref differs depending on the numerical models shown below.

The new empirical model shown in Eq. (6) was proposed using assumptions mentioned above together with assumption (e).

(e) Velocity components are functions of radius and height only (f(r)×f(z)).

In the proposed model, the maximum radial flow was found at the ground ($\bar{r}$=1 and $\bar{z}$=0), reflecting the results of field measurement and wind tunnel experiment, i.e. where the strongest inflow was concentrated very near the ground. The radial velocity was firstly proposed, and the vertical velocity was obtained from the radial velocity (Eq. (6a)) and Eq.(4). The tangential velocity can be obtained by inserting radial and vertical velocities into Eq.(2). There are three parameters in the proposed model, and the velocity components show clear variations with radius and height, overcoming the shortcomings of existing numerical models. The radial and vertical profiles of velocity components were compared with the results of field measurements, wind tunnel experiment and computational fluid dynamics and shows good agreement with them. Detail discussions on the proposed model can be found in Kim and Tamura (2020b).

$$\bar{U} = \frac{-2\bar{r}(1-\bar{z}^2)}{(1+\bar{r}^2)(1+\bar{z}^2)^2} \quad (6a)$$

$$\bar{V} = \frac{C\bar{r}^{2\alpha-1}\bar{z}^{\alpha}}{(1+\bar{r}^2)^{\alpha}(1+\bar{z}^2)^{\alpha}} \quad (6b)$$

$$\bar{W} = \frac{4\zeta\bar{z}}{(1+\bar{r}^2)^2(1+\bar{z}^2)} \quad (6c)$$

where, velocity components are normalized by the maximum radial velocity Umax as in the Baker model, and radius and height are normalized by the reference radius and reference height. ζ is defined as zref / rref. C = 4 and α = 1 (Kim and Tamura, 2020b).

In the present study, the Modified Rankine model, the Burgers-Rott model, the Kou-Wen model, the Fujita model, and the Baker model were used for comparison. Their numerical expressions were briefly introduced as follows (Kim and Matsui, 2017; Kim and Tamura, 2020b).

Modified Rankine model

$$\bar{V} = \begin{cases} \bar{r} & (\bar{r} < 1) \\ \bar{r}^{-\varepsilon} & (\bar{r} \geq 1) \end{cases} \quad (7a)$$

$$\bar{U} = -0.5\bar{V} \quad (7b)$$

$$\bar{W} = 0.67\bar{V} \quad (7c)$$

where, U, V, and W are normalized by the maximum tangential velocity Vmax and ε is a decay index expressing the degree of decrease in the outer region. It seems that ε ranges from 0.4 to 0.8 (Kim and Matsui, 2017), and ε of 0.5 was used hereafter.

Burgers-Rott model

$$\bar{U} = -a\frac{r_{ref}}{V_{max}}\bar{r} \quad (8a)$$

$$\bar{V} = \frac{1}{K_{RB2}}\frac{1}{\bar{r}}\{1 - exp(-K_{RB1}\bar{r}^2)\} \quad (8b)$$

$$\bar{W} = 2a\frac{z_{ref}}{V_{max}}\bar{z} \quad (8c)$$

where, velocity components are normalized by the maximum tangential velocity Vmax, a is the velocity gradient (1/s, 0.005/s for eddy viscosity of 5m^2/s), and KBR1 and KRB2 are 1.26 and 0.72, respectively.

Kou-Wen model

$$\delta = \delta_\infty\{1 - exp(-0.5\bar{r}_o^2)\} \quad (9a)$$

$$\bar{U}_o = 0 \quad (9b)$$

$$\bar{V}_o = \frac{1.4}{\bar{r}_o}\{1 - exp(-1.256\bar{r}_o^2)\} \quad (9c)$$

$$\bar{W}_o = 93\bar{r}_o^3 exp(-5\bar{r}_o) \quad (9d)$$

$$\bar{U}_i = \bar{V}_o\{0.672exp(-\pi\bar{\eta})sin(\pi(\bar{b}+1)\bar{\eta})\} \quad (9e)$$

$$\bar{V}_i = \bar{V}_o\{1 - exp(-\pi\bar{\eta})cos(2\pi\bar{b}\bar{\eta})\} \quad (9f)$$

$$\bar{W}_o = \bar{W}_o\{1 - exp(-\pi\bar{\eta})cos(2\pi\bar{b}\bar{\eta})\} \quad (9g)$$

$$\bar{\eta} = \frac{z}{\delta} \quad (9h)$$

$$\bar{b} = 1.2exp(-0.8\bar{r}_o^4) \quad (9i)$$

where, reference velocity and reference radius are the maximum tangential velocity and its radius outside the boundary layer Vmaxo and rco, δ is the boundary layer thickness, and δ∞ is the boundary layer thickness at infinity (δ∞ = 350m was assumed hereafter).

Baker model

$$\bar{U} = \frac{-4\bar{r}\bar{z}}{(1+\bar{r}^2)(1+\bar{z}^2)} \quad (10a)$$

$$\bar{V} = \frac{2.89S\bar{r}\ln(1+\bar{z}^2)}{(1+\bar{r}^2)} \quad (10b)$$

$$\bar{W} = \frac{4\zeta\ln(1+\bar{z}^2)}{(1+\bar{r}^2)^2} \quad (10c)$$

where, velocity components are normalized by the maximum radial velocity Umax, and radius and height are normalized by the reference radius and reference height, respectively. ζ is defined as zref / rref. S = 1.

3. LOAD EFFECTS ON LOW-RISE BUILDING AND AERODYNAMIC FORCES ON TALL BUILDING

In the Section 3, using the proposed model, loading effects induced by surface pressures on low-rise building and quasi-steady aerodynamic force coefficients on tall building were calculated and compared with those obtained from existing numerical models mentioned above.

3.1 PEAK NORMAL STRESSES ON COLUMN ON LOW-RISE BUILDING

Fig.2 shows the locations of tornado passage and schematics of the analytical low-rise building used in the present study. Tornado properties including moving velocity Umov, reference wind speed Uref, reference radius rref and height zref were assumed considering the tornado properties in Japan, and 1,000m length in X-direction and 400m in Y-direction was set to the area of calculation. Considering the reference radius of 50m, they correspond to 20 times of rref and 8 times of rref respectively. A typical low-rise building ($B \times D \times H$ = 20m × 20m × 10m) was assumed, having square cross-section columns and beams. The columns were assumed to be installed at each corner, and the beams were assumed to be stiff. Column size was determined such that tip displacement angle is less than 1/200. The peak normal stresses in columns were caused by the resultant effects of surface pressures, and no dead load and no live load were applied, so that the effects of wind force combinations only were evaluated.

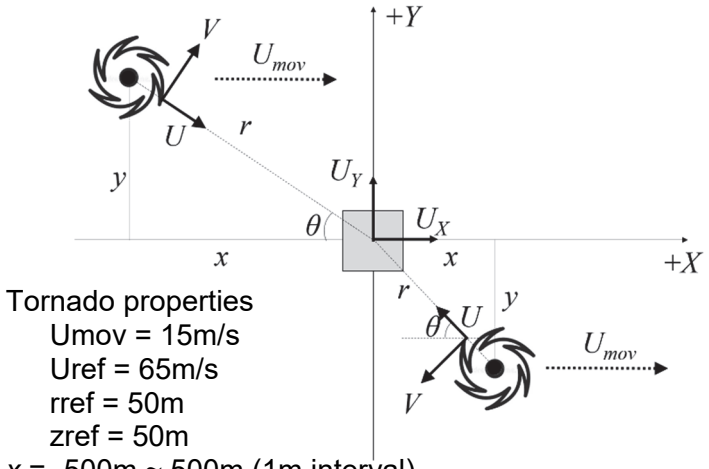

(a) Location of tornado passage

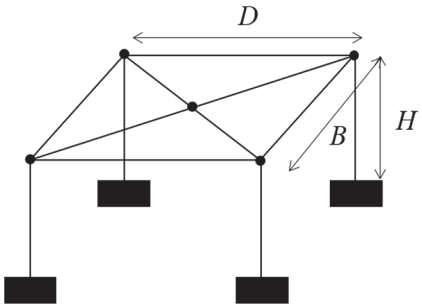

(b) Analytical low-rise building ($B \times D \times H$ = 20m × 20m × 10m)

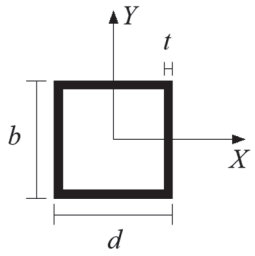

$b = d$ = 0.5m
t = 0.02m
A = 0.0384m^2
$ZX = ZY$ = 0.005908m^3

(c) Column properties

Fig.2 Locations of tornado passage and analytical low-rise building.

Fig.3 shows a contribution of each stress component where the maximum total stress σtotal occurs for several models. For all models, a stress in Y-direction σY is the largest, and a stress in Z-direction σZ is the smallest. σZ was resulted only from the vertical velocity, implying that the vertical velocity could be ignored in the calculation of tornado-induced load by the surface pressure. However, note that impact load by wind-borne debris should also be considered in the tornado-resistant design, and in the calculation of impact load by wind-borne debris, the vertical velocity plays an important role. The contribution of σY to σtotal of the Modified Rankine and Kuo-Wen model is very large and that of the Baker model is the smallest in the present study. Quite strange variation was found for the Kuo-Wen model, which comes from the existence of a boundary layer in the tornado vortex.

Distributions of total stress σtotal for various numerical models were shown in Fig.4 for the ranges of y/rref ≤ ±4 and x/rref ≤ ±4. Black star in the contour is the point where the maximum total stress σ_{total} occurred, and white dotted line means a area for ±1 rref. Note that contribution of each stress component to the total stress shown in Fig.3 was the radial profile at this point. The maximum total stress was found on the positive y side on the ±1 rref for all models. But, the maximum total stress of the Modified Rankine, Fujita, and the present model was found at positive x and positive y direction (quadrant I plane). The Burgers-Rott and Kuo-Wen model show their maximum value on a positive y axis, and the Baker model shows its maximum value almost on the positive x axis. Again, quite strange and unrealistic variation was found for the Kuo-Wen model, which comes from the existence of a boundary layer in the tornado vortex. The total stress obtained from the Baker model is significantly small when compared with other models, but the situation is totally different for the aerodynamic forces on tall building discussed in Section 3.2.

Fig.5 shows the comparison of the maximum total stress which is expressed as a ratio to that of the Modified Rankine model. The maximum total stress of the Modified Rankine model is σtotal,Rankine ≈ 61kN/cm^2, and the smallest one is found for the Baker model, which is only 20% of the Modified Rankine model. The maximum total stresses of the Burgers-Rott, Kuo-Wen, Fujita and the present models show similar value, corresponding to almost 80% of that of the Modified Rankine model.

Note that in the present work, the dimensions of peak normal stresses themselves are not very meaningful. Relative comparison, ratio to that of the Modified Rankine model, needs to be paid attention to.

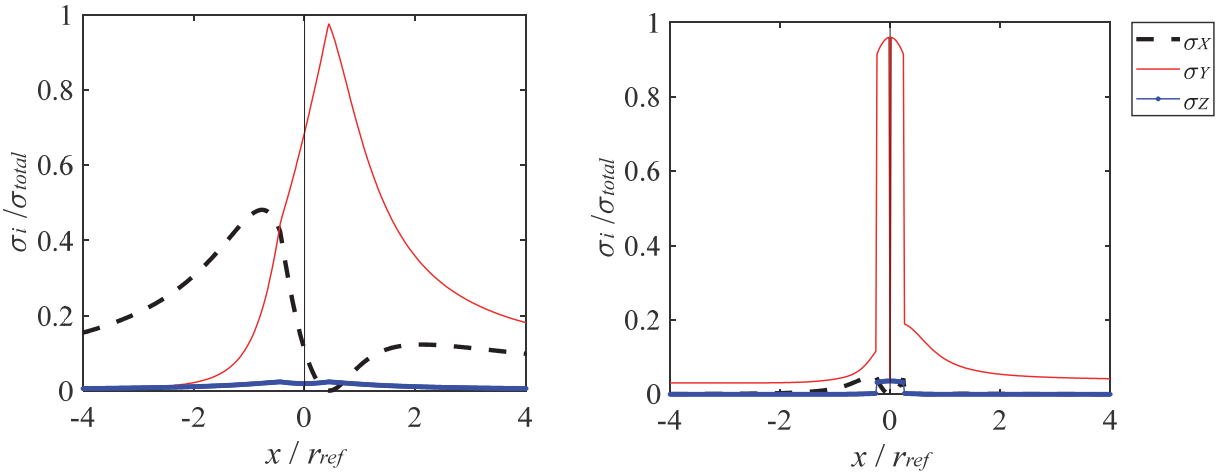

(a) Rankine model (b) Kuo-Wen model

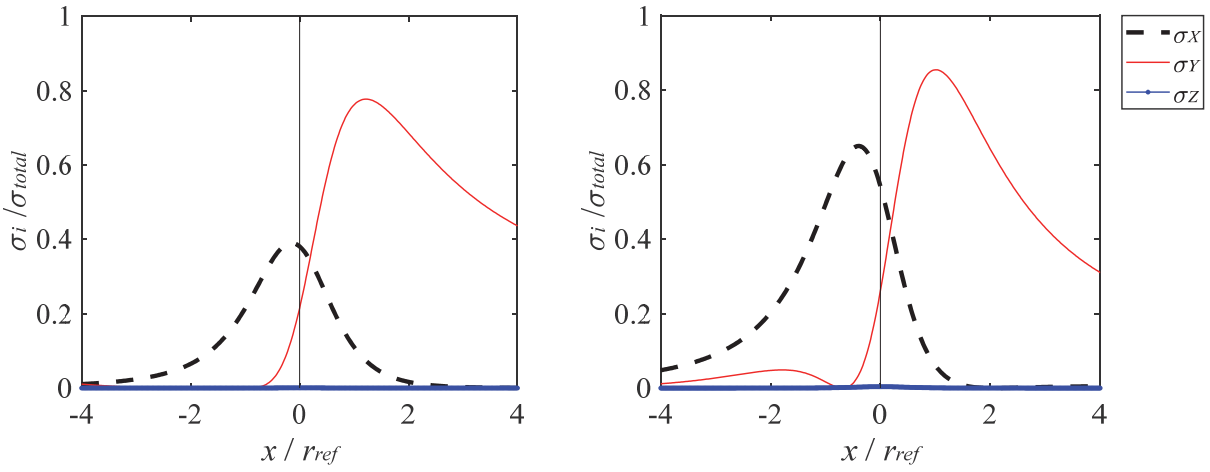

(c) Baker model (d) Present model

Fig.3 Contribution of each stress component where the maximum total stress σtotal occurs.

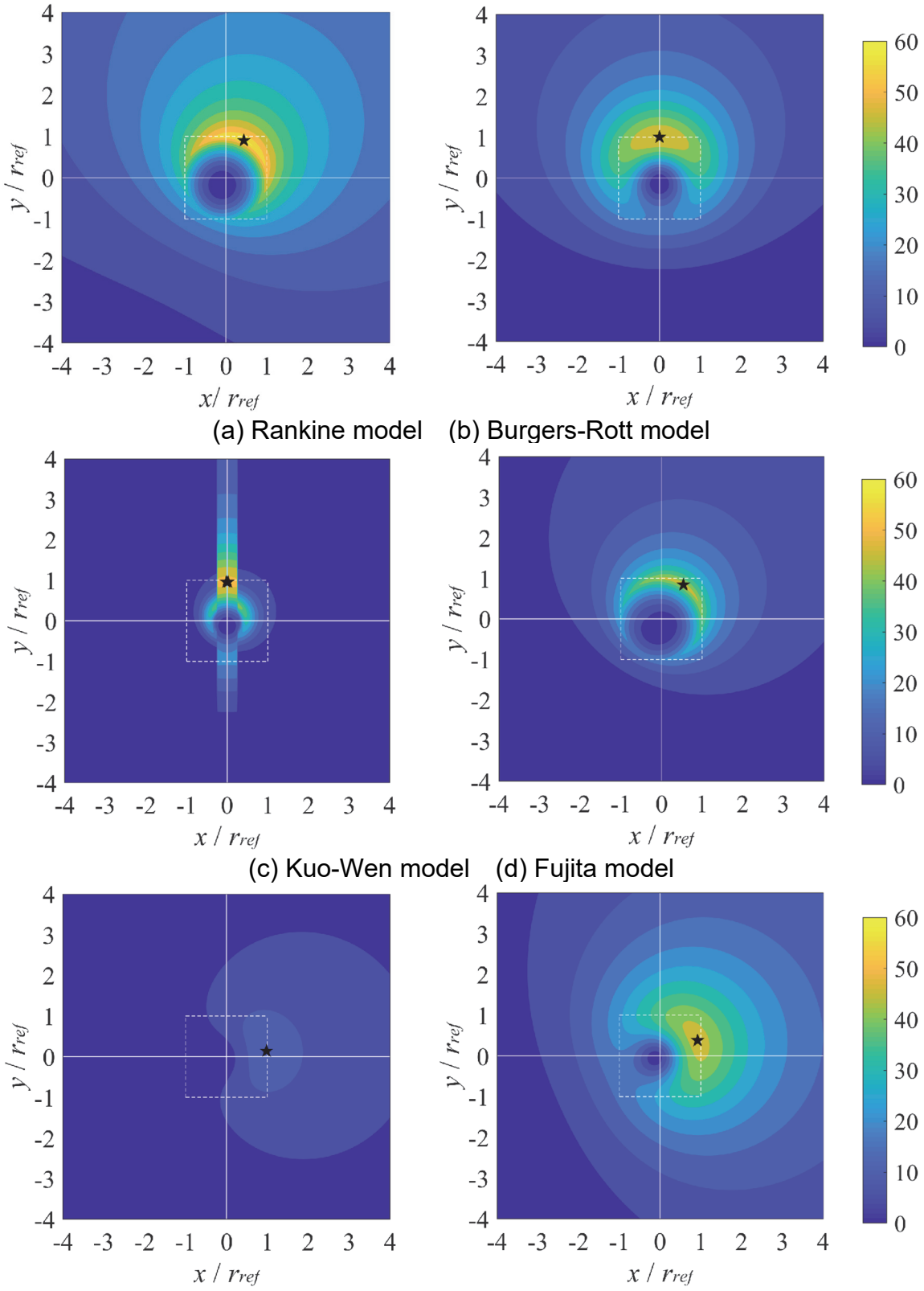

(a) Rankine model (b) Burgers-Rott model

(c) Kuo-Wen model (d) Fujita model

(e) Baker model (f) Present model

Fig.4 Distribution of total stress σtotal for various numerical models (kN/cm^2).

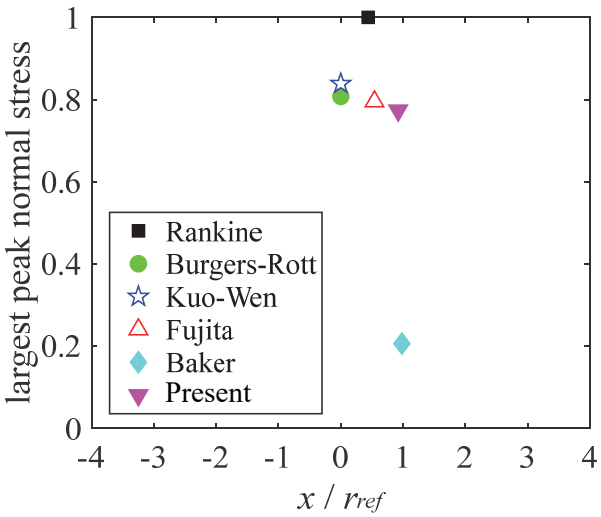

Fig.5 Comparison of the maximum total stress (ratio to the Rankine model, $\sigma_{total,Rankine} \approx 61 kN/cm^2$).

3.2 AERODYNAMIC FORCES ON TALL BUILDING

Simple quasi-steady aerodynamic forces on tall buildings were investigated analytically. Fig.6 shows schematics of relative positions of tornado and building section, and tornado-induced aerodynamic forces. In the present study, the tornado was assumed to pass through the center of the building along the X-axis. The tornado-induced wind effect was larger when a tornado passed the left side of the building (upper side in Fig.6) than that when it passed the right side (lower side in Fig.6). Assuming the tornado passes through the center of the building gives an intermediate wind effect (Kim, 2018).

The resulting aerodynamic forces FD(h) and FL(h) at elevation h can be defined by Eq.(11). In the present study, a building with dimensions B × D × H = 30m × 45m × 250m was considered, and its quasi-steady force coefficients and their derivatives were assumed to be CD = 1.0, CL = –0.1, CD´= –1.1, CL´ = 2.2. Turbulence intensities in the r and θ directions were assumed to be the same as those in the X and Y directions, and IX (=uX/UX) and IY (uY/UY) of 10% (IX = IY = 10%) were assumed tentatively.

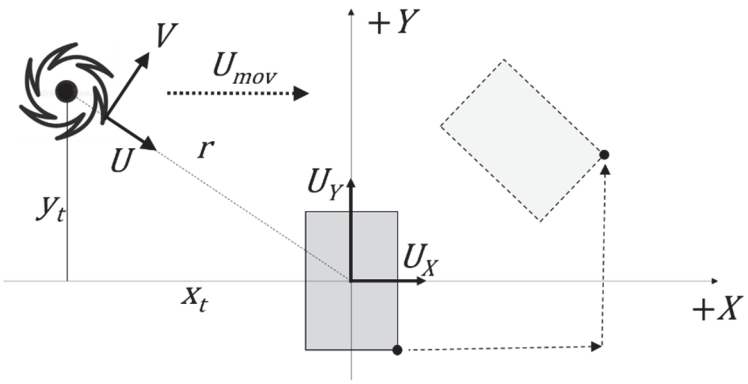

(a) Relative position of tornado and building

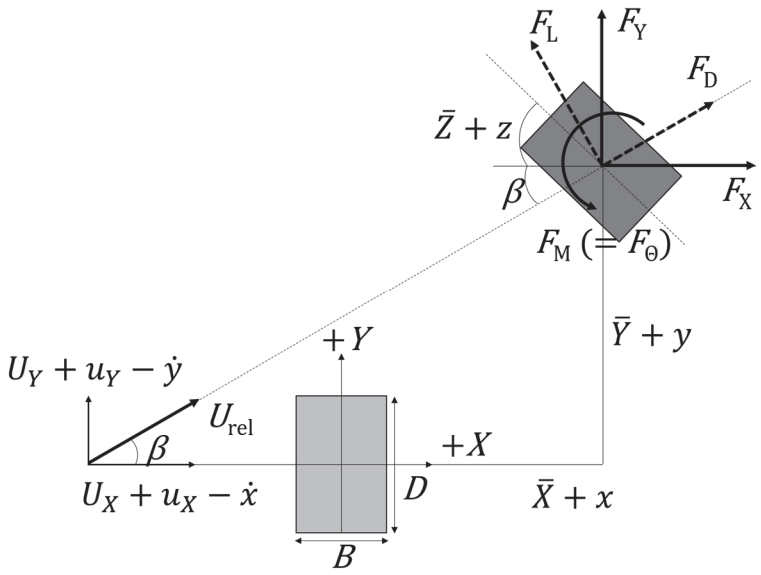

(b) Aerodynamic forces on building

Fig.6 Schematics of tornado and building and tornado-induced aerodynamic forces (Umov = 15m/s, Uref = 65m/s, rref = 50m, zref = 50m).

$$F_D(h)=\frac{1}{2}\rho D\Bigg[C_D\left(U_X(h)^2+U_Y(h)^2\right)+U_X(h)^2\left\{C_D\left(\frac{2u_X(h)}{U_X(h)}\right)+C_D'\beta\left(1+\frac{2u_X(h)}{U_X(h)}\right)\right\}+U_Y(h)^2\left\{C_D\left(\frac{2u_Y(h)}{U_Y(h)}\right)+C_D'\beta\left(1+\frac{2u_Y(h)}{U_Y(h)}\right)\right\}\Bigg] \quad (11a)$$

$$F_L(h)=\frac{1}{2}\rho D\Bigg[C_L\left(U_X(h)^2+U_Y(h)^2\right)+U_X(h)^2\left\{C_L\left(\frac{2u_X(h)}{U_X(h)}\right)+C_L'\beta\left(1+\frac{2u_X(h)}{U_X(h)}\right)\right\}+U_Y(h)^2\left\{C_L\left(\frac{2u_Y(h)}{U_Y(h)}\right)+C_L'\beta\left(1+\frac{2u_Y(h)}{U_Y(h)}\right)\right\}\Bigg] \quad (11b)$$

Fig.7 compares the largest aerodynamic force coefficients (Kim and Tamura, 2020a). The Kuo-Wen model shows the largest CFX, and the CFX of the Burgers-Rott model and the present model are similar. For CFY, the modified Rankine model and the Kuo-Wen model show similar larger values, while the Burgers-Rott model shows the smallest value. The largest aerodynamic force coefficients of the present model show values intermediate among the other models. Note that the largest aerodynamic force

coefficients of the Baker model are not shown, because they are much larger than those of other numerical models (about 19 times larger on average).

Fig.8 shows the vertical profile where the largest aerodynamic force coefficients shown in Figure 10 occur (Kim and Tamura, 2020a). The largest value of CFX occurs slightly below h/zref = 1 for the Kuo-Wen model (h/zref = 0.8) and the present model (h/zref = 0.9) and the largest CFY occurs at the height of h/zref = 0.8 for the Kuo-Wen model, while that for the present model occurs near the ground which is not shown here. As mentioned before, the vertical profiles of the modified Rankine model and the Burgers-Rott model are constant, and the aerodynamic force coefficients of the Baker model increase rapidly with height.

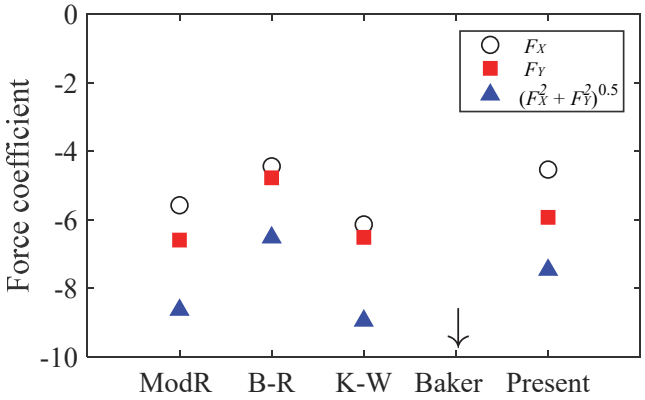

Fig.7 Comparison of largest aerodynamic force coefficients (For the Baker model, CFX: –110.6, CFY: –98.7) (Kim and Tamura, 2020a).

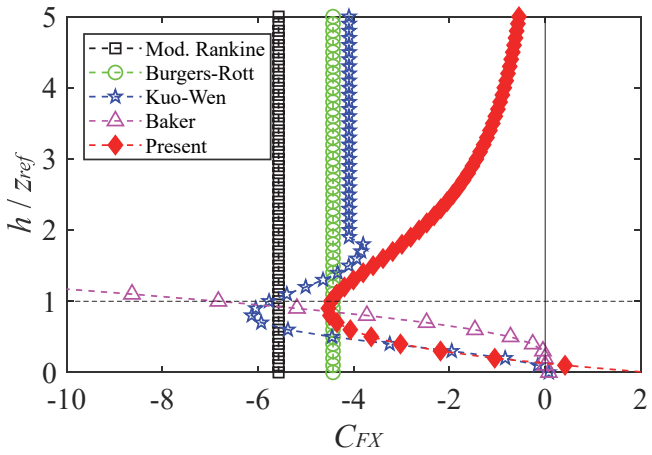

Fig.8 Vertical profiles of CFX where largest aerodynamic force coefficients occur (Kim and Tamura, 2020a).

The results shown before were obtained from the conditions of IX = IY = 0.1, Umov = 15m/s, Uref = 65m/s, rref = 50m and zref = 50m, and the effects of turbulence intensity IX and IY, moving velocity Umov, reference velocity Uref, reference radius rref and reference height zref on aerodynamic force coefficients were shown in Fig.9 (Kim and Tamura, 2020a). Turbulence intensities IX and IY increased up to 90%, keeping IX = IY (IX = IY = 0, 0.1, ⋯, 0.9). As shown in Fig.9(a), aerodynamic force coefficients

increase linearly with increasing turbulence intensity for CFX, and similar trend was found for CFY. Aerodynamic force coefficients increase by roughly 10% when the turbulence intensities increase by 10%. The effects of reference velocity Uref was shown in Fig. 9(b). Reference velocity was changed from about 7m/s to 585m/s, setting the other parameters constant, and aerodynamic force coefficients were normalized by corresponding reference velocities. Aerodynamic force coefficients shown in Fig.9(b) decrease with increasing reference velocity up to roughly 30m/s and increase slightly with increasing reference velocity. CFY is generally larger than CFX, especially for the larger reference velocity. The opposite trend of moving velocity (Umov = 1.7m/s ~ 135m/s) was found as shown in Fig.9(c), still showing larger aerodynamic force coefficients in the Y direction. The effects of reference radius rref and reference height zref are shown in Fig.9(d) for fixed reference velocity and moving velocity. It is interesting that aerodynamic force coefficients were little influenced by the reference radius and reference height, showing almost constant values and trends. Aerodynamic force coefficients from the present model are shown in Fig.9, and the similar results were obtained for other numerical models.

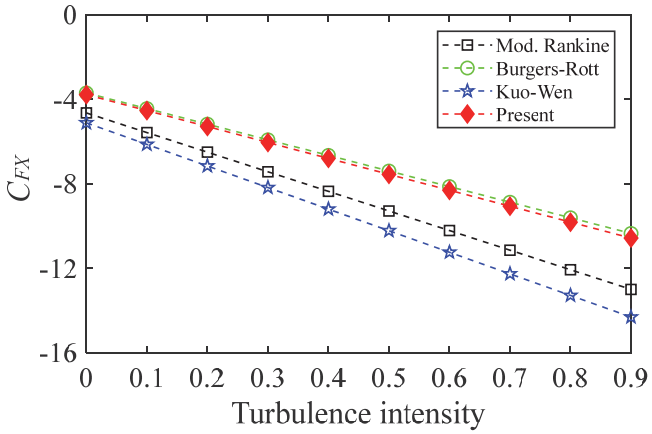

(a) Turbulence intensity on CFX

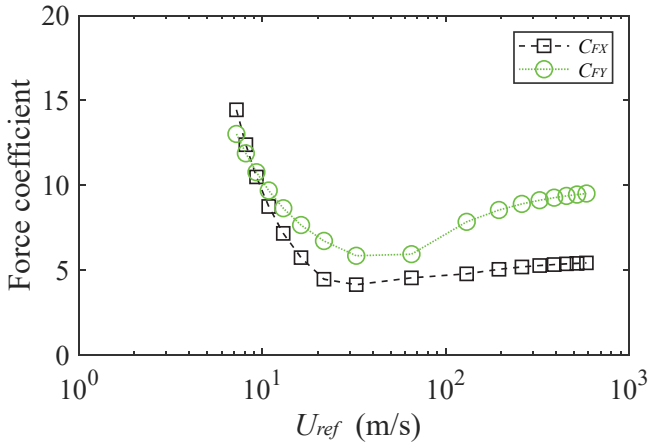

(b) Reference velocity

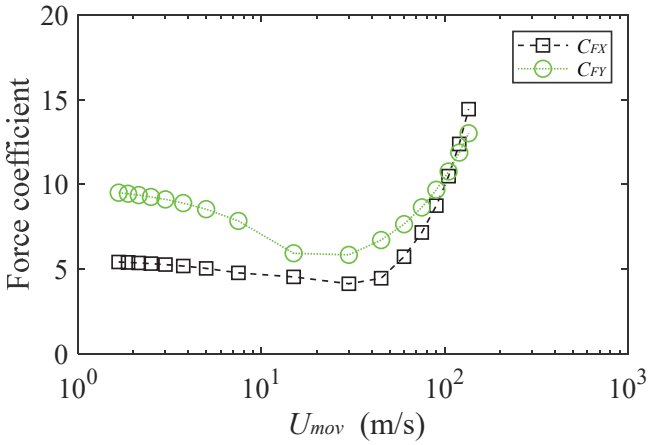

(c) Moving velocity

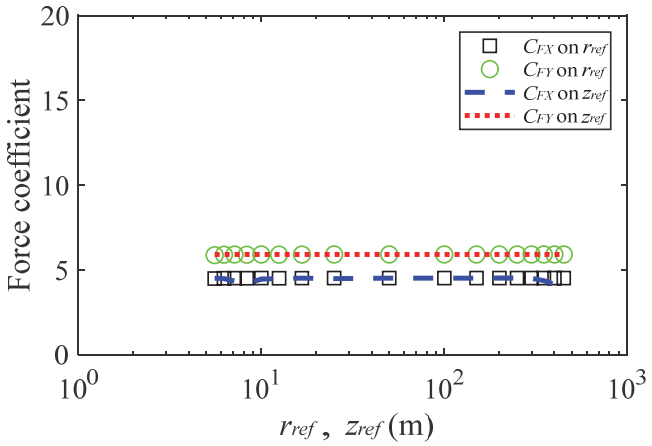

(d) Reference radius and reference height

Fig.9 Effects of turbulence intensity (CFX), reference velocity, moving velocity, reference radius and reference height on aerodynamic force coefficients (Kim and Tamura, 2020a).

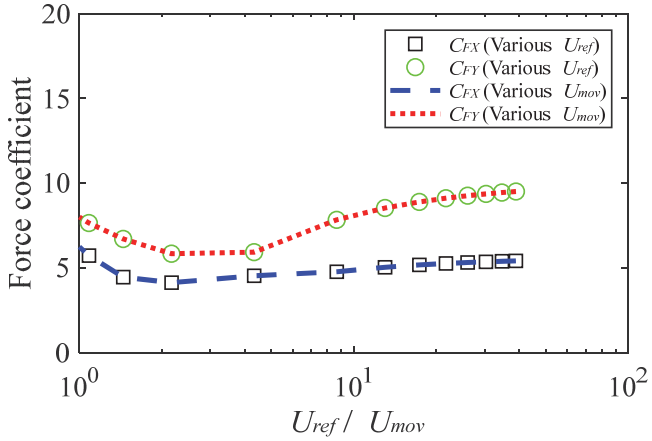

Fig.10 Combined effect of reference velocity and moving velocity on aerodynamic force coefficients for the present model (Kim and Tamura, 2020a).

The effects of reference velocity and moving velocity are shown separately in Fig.9, and the combined effect of reference velocity and moving velocity is shown in Fig.10, in which variation of aerodynamic force coefficients on a normalized velocity Uref/Umov ranging from 0.5 to 39 is shown for the present and modified Rankine models (Kim and Tamura, 2020a). It is quite interesting that aerodynamic force coefficients were well collapsed for the same normalized velocity Uref/Umov regardless of individual variations, implying that the combined effects of reference velocity and moving velocity are more important than the individual effects. Similarly, exactly the same vertical profiles were found at the same normalized velocities Uref/Umov.

4. CONCLUSIONS

A new empirical modeling for tornado vortex was proposed and load effects on low-rise building and aerodynamic forces on tall buildings were calculated and compared with those from several existing models.

Peak normal stresses on column on low-rise building were compared. The maximum total stress were found at positive y side near the reference radius for all numerical models. The maximum total stress of the Modified Rankine model was the largest, and that of the proposed model show similar value to other numerical models except the Baker model, showing almost 80% of that of the Modified Rankine model.

Aerodynamic force coefficients on tall building were calculated based on the simplified quasi-steady theory, which ignores the effects of flow distortion and size effect of disturbance in tornado vortex, and the results from the proposed model show similar values to most existing models, while those from the Baker model show much larger values. Aerodynamic force coefficients increased with increasing turbulence intensity and were found to depend mainly on reference velocity Uref and moving velocity Umov. However, they collapsed to one curve for the same Uref/Umov. The effects of reference radius and reference height were found to be small.

ACKNOWLEDGE

This study was supported by The Taisei Foundation. The authors gratefully acknowledge this support. Helpful discussions with Dr. C.J. Baker at the University of Birmingham are gratefully acknowledged.

REFERENCES

Baker CJ, 2016, Debris flight in tornadoes, 8th International Colloquium on Bluff Body Aerodynamics and Applications, Boston, USA.

Church CR, Snow JT, Baker GL, Agee EM, 1979, Characteristics of tornado-like vortices as a function of swirl ratio: A laboratory investigation, Journal of the Atmospheric Science 36, pp. 1755 – 1776.

Kim YC, 2018, Comparison of tornadic wind loads from various numerical expressions, International Workshop on Wind-Related Disasters and Mitigation, Paper ID 57, Sendai, Japan

Kim YC, Matsui M, 2017, Analytical and empirical models of tornado vortices: A comparative study, Journal of Wind Engineering & Industrial Aerodynamics 171, pp. 230-247.

Kim YC, Tamura Y, 2020a, Empirical modeling of tornado vortex and its aerodynamic effect of a typical rectangular-type high building, Submitted to Journal of Fluids and Structures.

Kim YC, Tamura Y, 2020b, Numerical modeling of one-cell tornado vortices, Journal of Structural Engineering, Architectural Institute of Japan 66, Paper ID 27.